Dalton Transactions

ROYAL SOCIETY OF CHEMISTRY

PAPER

View Article Online
View Journal

Cite this: DOI: 10.1039/d0dt01688h

UiO-66 as a catalyst for hydrogen production *via* the hydrolysis of sodium borohydride

Hani Nasser Abdelhamid

The exploration of a highly efficient catalyst for the hydrolysis of sodium borohydride ($NaBH_4$) is a valuable step toward a hydrogen economy. UiO-66 (Universitetet i Oslo) was synthesized *via* a solvothermal method using acetic acid as a modulator. The material was characterized using X-ray diffraction (XRD), nitrogen adsorption–desorption isotherms, Fourier transform infrared (FT-IR) spectroscopy, thermogravimetric analysis (TGA), temperature-programmed desorption (TPD), and transmission electron microscopy (TEM). Data analysis reveals the formation of a pure and highly crystalline phase of UiO-66 with the Brunauer–Emmett–Teller (BET) and Langmuir specific surface areas of 1125 $m^2\ g^{-1}$, and 1250 $m^2\ g^{-1}$, respectively. UiO-66 was analysed as a catalyst for hydrogen generation *via* the hydrolysis of $NaBH_4$. The effect of the $NaBH_4$ amount and catalyst loading was investigated. The reaction time decreased with an increase of the amount of $NaBH_4$ or UiO-66. UiO-66 exhibited an average hydrogen generation rate of 6200 mL $min^{-1}\ g^{-1}$. The high catalytic performance of UiO-66 could be due to its large surface area and acidic sites. The results suggested that UiO-66 showed high potential to catalyze the hydrogen production *via* the hydrolysis of hydrides.

Received 10th May 2020,
Accepted 22nd June 2020

DOI: 10.1039/d0dt01688h

rsc.li/dalton

Introduction

Hydrogen (H_2) gas is a renewable and sustainable clean energy source with high combustion efficiency, and environmentally friendly by-products.[1,2] It can be used as a fuel with a specific energy of 120 MJ kg^{-1} which is higher than those of diesel and gasoline (46 MJ kg^{-1}). The production of hydrogen can be achieved using phototrophic microorganisms[1] and several methods such as biomass gasification,[3] solar hydrogen,[4] and water oxidation.[5] Among these methods, the hydrolysis of hydrides such as sodium borohydride ($NaBH_4$) offers several advantages.[6] The hydrolysis process is well known for many applications in energy and materials science. $NaBH_4$ has high gravimetric and volumetric capacities compared to other metal hydrides. It serves as a water-splitting agent since half of the produced hydrogen is produced from water. The hydrolysis process is useful for low energy demand applications such as unmanned airplanes, and small portable devices.[6] However, a catalyst is required to improve and control the rate of the self-hydrolysis process.[6]

Metal–organic frameworks (MOFs) are self-assembled coordination polymers with high porosity and large surface areas.[7–13] They have been applied in various methods/techniques for the production of hydrogen.[14,15] Several MOFs such as zeolitic imidazolate frameworks (ZIF-8),[16–18] partially decomposed ZIF-67 supported Pd nanoclusters (Pd/PD-ZIF-67),[19] and copper-1,4-benzenedicarboxylate (CuBDC)[20] were reported as catalysts for hydrogen production *via* the hydrolysis of $NaBH_4$. UiO-66 (Universitetet i Oslo) is an archetypal MOF with a high specific surface area and high chemical and thermal stability[21–23] and is amenable to further modifications.[24] It can be easily synthesized in the lab with great potential for commercialization. UiO-66 was used for photodynamic therapy,[25] drug delivery,[26] CO_2 adsorption,[27] metal adsorption,[28] dye adsorption,[29] and separation,[30] and as a probe for the detection of hydrazine.[31] It is used as a catalyst or support for a catalyst. UiO-66 was also used for the selective transformation of alkynes into alkenes,[32] photoreduction of CO_2 to formate,[33] and hydrodeoxygenation of vanillin.[34] It can be used as a support for the NiFePd catalyst which exhibited efficient catalytic performance for the generation of hydrogen from hydrous hydrazine in an alkaline solution.[35]

Herein, UiO-66 was synthesized and applied as a catalyst for hydrogen generation *via* the hydrolysis of $NaBH_4$. A solvothermal method with acetic acid as a modulator was used to synthesise UiO-66. The material was characterized using X-ray diffraction (XRD), transmission electron microscopy (TEM), nitrogen adsorption–desorption isotherms, thermogravimetric analysis (TGA), temperature-programmed desorption (TPD), and Fourier transform infrared (FT-IR) spectroscopy. A pure crystalline phase of UiO-66 is obtained with a specific surface area of Brunauer–Emmett–Teller (BET), and Langmuir of 1125 $m^2\ g^{-1}$, and 1250 $m^2\ g^{-1}$, respectively. It exhibited a maximum hydrogen generation rate (HGR) of 12400 mL min^{-1}

Advanced Multifunctional Materials Laboratory, Department of Chemistry, Assiut University, 71516 Assiut, Egypt. E-mail: hany.abdelhamid@aun.edu.eg

g^{-1} with an average HGR of 6200 mL min^{-1} g^{-1} using 5 mg of the catalyst at 30 °C. The results may lead to further exploration of the applications of MOFs as catalysts for the generation of hydrogen using chemical reagents such as $NaBH_4$.

Materials and methods

Acetic acid, dimethylformamide (DMF), 1,4-benzenedicarboxylic acid (BDC), and $ZrOCl_2$ were purchased from Sigma-Aldrich (Germany). All the chemical reagents were used without further purification.

Synthesis of UiO-66

$ZrOCl_2$ (750 mg), 1,4-benzenedicarboxylic acid (BDC, 740 mg), and acetic acid (4 mL) were mixed in DMF (90 mL) using ultrasonication for 30 min. The solution was transferred to a Teflon-lined stainless steel autoclave (100 mL) and heated at 120 °C for 24 h. The reaction solution was cooled down to room temperature and washed three times using DMF (3 × 30 mL), and ethanol (3 × 30 mL). The sample was dried in an oven overnight (85 °C).

Characterization methods

The morphology of UiO-66 was investigated using a transmission electron microscope (TEM, JEOL 2100F). The crystal phase of the sample was determined using a powder X-ray diffractometer (XRD Phillips PW1700 (Rockville, USA)) with Cu K_α radiation (λ = 0.15405 nm) at an accelerating voltage and current of 40 kV and 40 mA, respectively.[36] The specific surface areas (BET and Langmuir) were measured using N_2 adsorption–desorption isotherms (at 77 K) by employing an ASAP2000 surface area analyzer (Micrometric, UK). The pore size distribution was evaluated using the BJH (Barrett, Joyner, and Halenda) method. The sample was degassed at 120 °C under vacuum for 3 h. The Fourier transform infrared spectra (FT-IR) of UiO-66 were measured using a Nicolet spectrophotometer (model6700). The thermogravimetric analysis (TGA) of UiO-66 was performed using a TA 60 thermal analyzer apparatus (Shimadzu, Japan).

The catalytic reaction for the hydrolysis of $NaBH_4$

The hydrolysis of $NaBH_4$ was performed at 30 °C using UiO-66 of 5, 10, and 50 mg. $NaBH_4$ of 0.19 g, 0.34 g, 1 g, 2 g, and 3 g was added to 100 mL of water (corresponding to 0.19 wt%, 0.34 wt%, 1 wt%, 2 wt%, and 3 wt%). Then, a catalyst UiO-66 was added. The reaction solution was stirred at 1000 rpm. The generated volume of hydrogen was measured using the water displacement method.[20]

The effect of temperature was evaluated at temperatures of 30 °C, 50 °C, and 60 °C. The amount of UiO-66 was 50 mg. Different amounts of $NaBH_4$ were employed such as 0.34 g, 1 g, and 2 g. The experimental setups were the same as mentioned above.

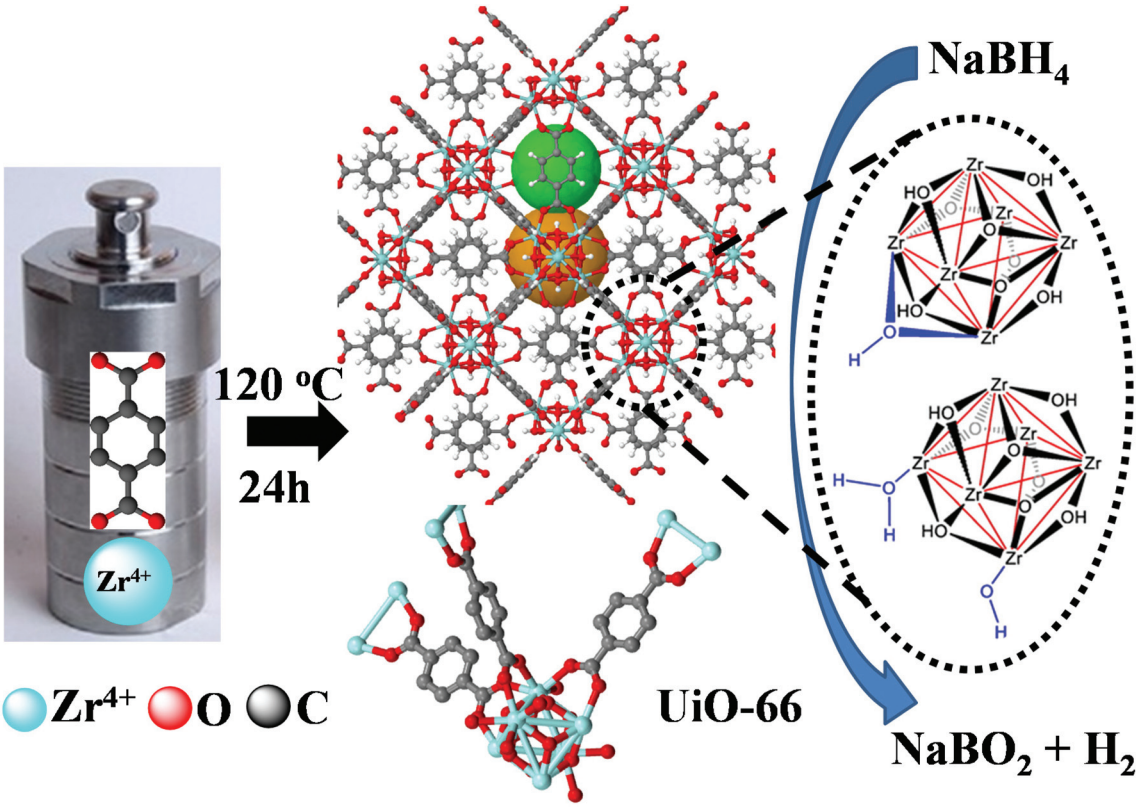

Fig. 1 Solvothermal synthesis of UiO-66; its crystal structure and applications for the hydrolysis of $NaBH_4$; the orange and green spheres refer to the primary pore size and the secondary pore size, respectively. Zirconium clusters are presented.

Acidity determination for UiO-66

Thermal analysis was used to determine the surface acidity of UiO-66 *via* temperature-programmed desorption (TPD). Basic probe pyridine (PY) was used. Briefly, the PY molecules were adsorbed onto 100 mg of UiO-66. The material after adsorption was analyzed using thermogravimetric analysis (TGA, a TA 60 thermal analyzer apparatus, Shimadzu, Japan) in the gas feed at a total flow rate of 50 mL min^{-1}.

Results and discussion

Material Characterization

The solvothermal synthesis of UiO-66 was achieved using DMF as a solvent leading to the formation of a white precipitate (Fig. 1). The XRD pattern of the formed precipitate was compared to the simulated XRD pattern of UiO-66 (Fig. 2a). The XRD pattern of the synthesized material and the simulated XRD pattern of UiO-66 matched very well indicating that a pure phase of UiO-66 was obtained (Fig. 2a). The data reveal that UiO-66 exhibits high crystallinity. UiO-66 consists of $[Zr_6O_4(OH)_4]$ clusters linked by 1,4-benzenedicarboxylic acid linkers. The crystal structure reveals that UiO-66 is a porous material (Fig. 1). Thus, nitrogen adsorption–desorption was used to evaluate the material porosity (Fig. 2).

The porosity of UiO-66 was evaluated using the nitrogen adsorption–desorption isotherm (Fig. 2b). Data analysis revealed the BET and Langmuir specific surface areas of 1125, and 1250 m^2 g^{-1}, respectively. These values agree with the reported values of the BET surface area.[37] The pore size distribution using the BJH method was also evaluated as shown in Fig. 2c. Data analysis suggests a total pore volume of 0.5 cm^3 g^{-1} (Fig. 2c). The nitrogen adsorption–desorption isotherm confirms the successful synthesis of UiO-66 with a high surface area and large pore volume (Fig. 2).

The chemical functional groups of UiO-66 are characterized using FT-IR spectroscopy (Fig. 3a). The FT-IR spectrum of UiO-66 shows vibrational bands at a wavenumber in the range of 2922–2847 cm^{-1} corresponding to C–H (Fig. 3a). The spectrum displays strong bands in the 1700–1250 cm^{-1} range arising from the carboxylate groups and phenyl ring deformations. The symmetric and asymmetric peaks of C═O can be observed at 1656 cm^{-1} and 1385 cm^{-1}, respectively. The band at 403 cm^{-1} is assigned to the Zr–O bond vibrations. The bands at 603 cm^{-1} and 665 cm^{-1} correspond to the Zr–O stretching mode. The FT-IR data confirm the coordination bonds between the Zr nodes ($[Zr_6O_4(OH)_4]$) and carboxylic groups of the linker.

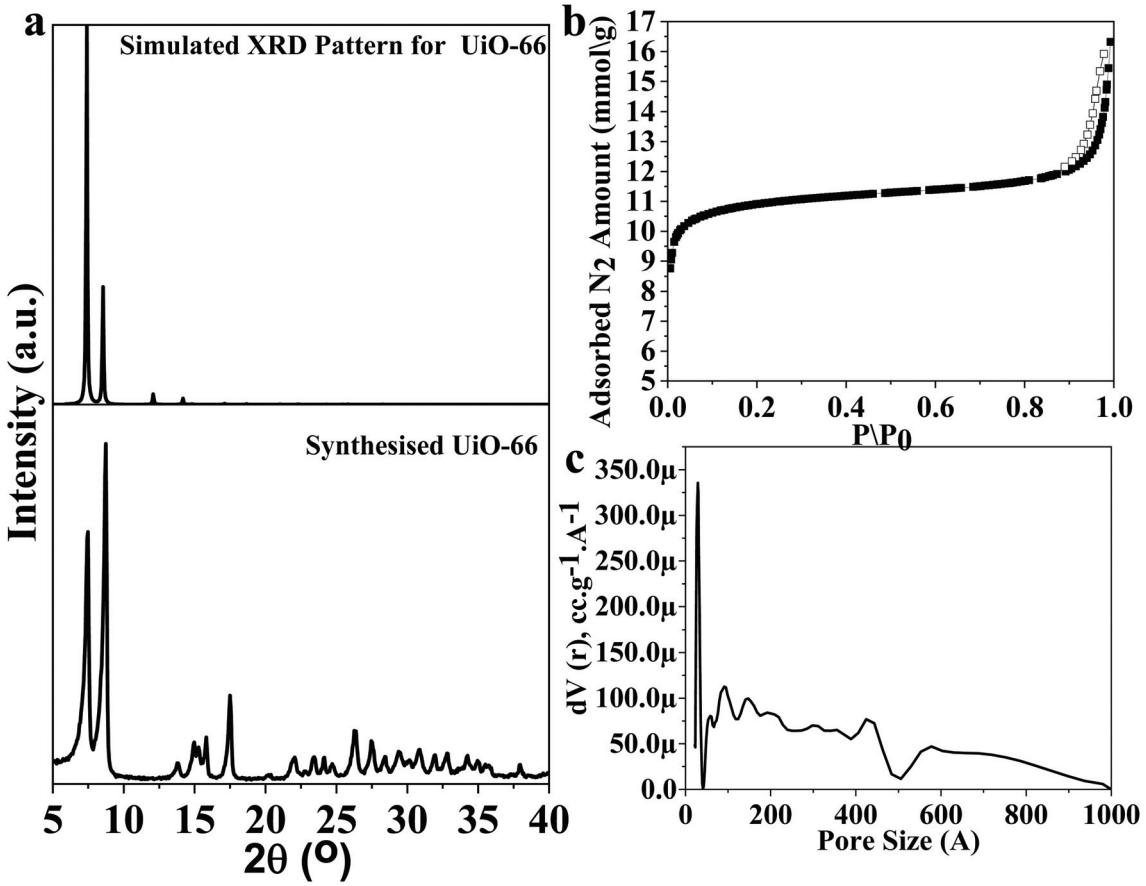

Fig. 2 Characterization of UiO-66 using (a) XRD and (b) N_2 adsorption (closed symbols)-desorption (open symbols) isotherms, and (c) the pore size distribution using the BJH method.

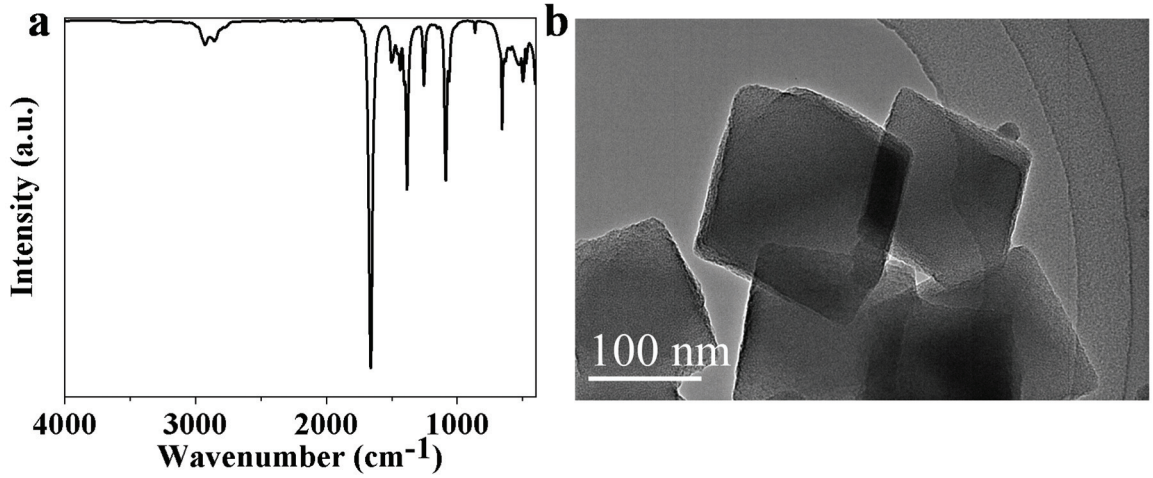

Fig. 3 (a) FT-IR spectrum and (b) TEM image of UiO-66.

The morphology and particle size of UiO-66 were determined using the TEM image (Fig. 2b). The TEM image of UiO-66 shows a crystal with a particle size of 175 nm (Fig. 3b). The UiO-66 crystals show an octahedral morphology (Fig. 3b). There is no observation of the extra crystal phase indicating that the synthesized material has high purity. This observation is consistent with the XRD data (Fig. 2a).

The thermal stability of UiO-66 was determined using the TGA curve (Fig. 4a). Fig. 4a shows three weight-loss steps. The first weight-loss step observed in the temperature range of 50–150 °C is due to the desorption of physisorbed molecules such as water. The second weight-loss step was observed in the temperature range of 150–350 °C. This weight loss is related to the thermal desorption of DMF or the dehydroxylation of the Zr nodes ($[Zr_6O_4(OH)_4]$).[38] The third weight lost step at 500 °C refers to the vaporization of the organic linker in the UiO-66 crystals. The TGA curve indicates that UiO-66 has thermal stability up to 500 °C (Fig. 4a). The residual material is ZrO_4 (found is 52% and calculated is 55% using the molecular formula $C_{48}H_{28}O_{32}Zr_6$, and formula weight 1664.06 g mol^{-1}). The TGA result confirms the high thermal stability of UiO-66 and reveals that the material has highly pure crystals of UiO-66.

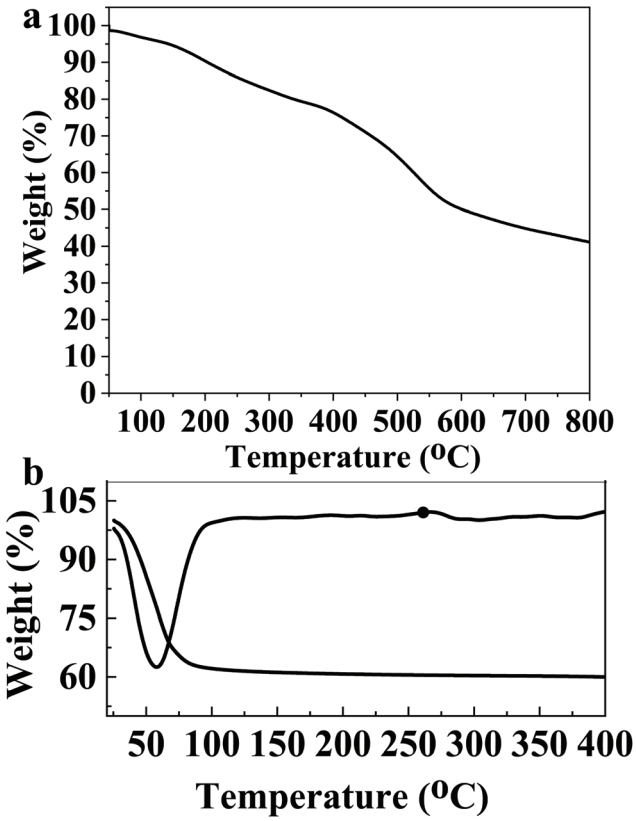

Fig. 4 Thermal analysis of UiO-66 using (a) TGA and (b) PY-TPD.

Application of UiO-66 for hydrogen generation *via* the hydrolysis of $NaBH_4$

The application of UiO-66 for hydrogen generation *via* the hydrolysis of $NaBH_4$ was investigated (Fig. 5 and 6). UiO-66 was selected because of the high surface area of its crystals. It has also acidic sites that can serve as active catalytic positions for the hydrolysis of $NaBH_4$. UiO-66 has a Zr_6 node with a fully reversible hydroxylation group (Fig. 1). The total number of acidic sites over the surface of UiO-66 was quantitatively evaluated using pyridine-TPD (Fig. 4b). The PY-TPD curve shows a weight loss at 58 °C for UiO-66 due to the weak acidic sites inside the frameworks. Data analysis shows the total acidic sites of the 0.210×10^{20} site m^{-2} catalyst.[39] Furthermore, the Zr node has a flexible coordinative state of the Zr^{4+} species. It is possible to have both the hydroxylated and dehydroxylated forms (Fig. 1).[40] UiO-66 offers the amphoteric nature *e.g.* acid-base pair properties.[41,42] Thus, it can be used as an effective catalyst for the hydrogen generation *via* the hydrolysis of $NaBH_4$.

The effect of UiO-66 loading on the hydrolysis of $NaBH_4$ was investigated as shown in Fig. 5. The volume of the gener-

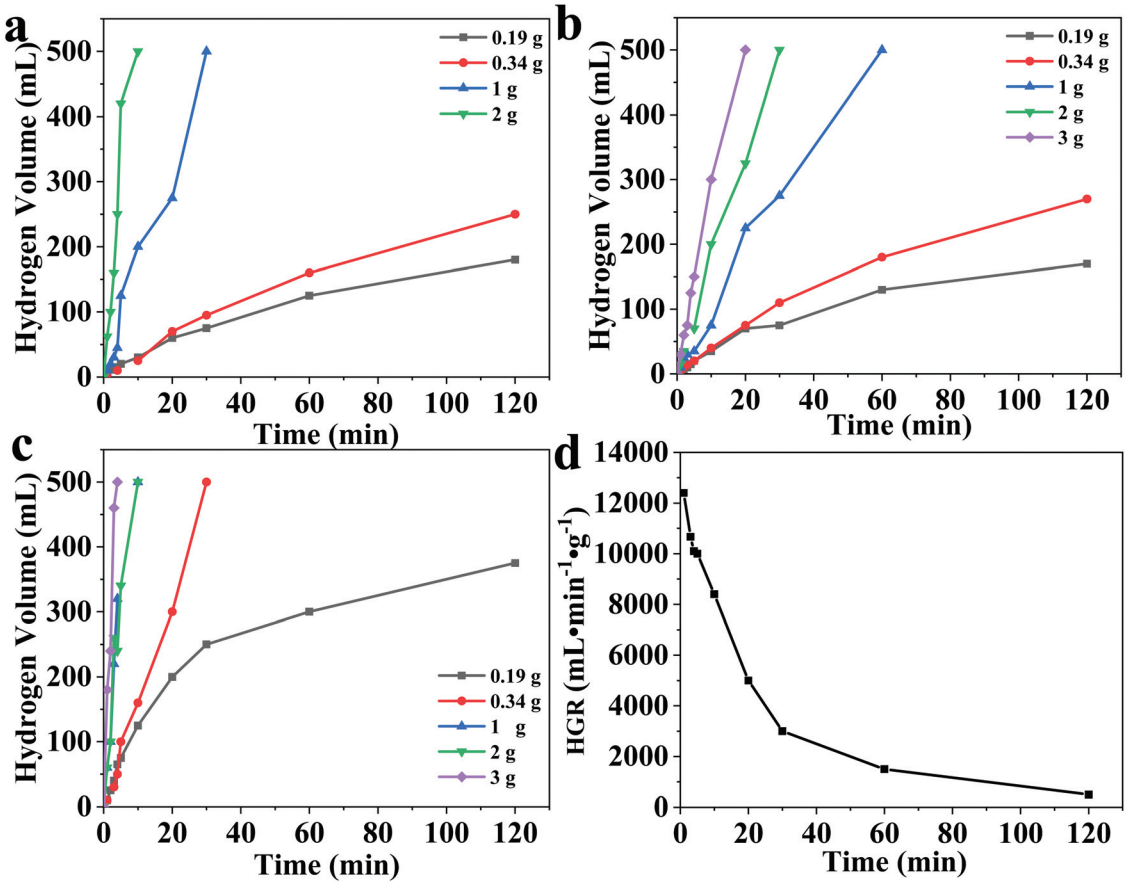

Fig. 5 The effect of UiO-66 loading on the hydrogen generation using (a) 5 mg, (b) 10 mg, and (c) 50 mg of UiO-66 at 30 °C. (d) hydrogen generation rate using 5 mg of UiO-66 and 2 wt% of $NaBH_4$.

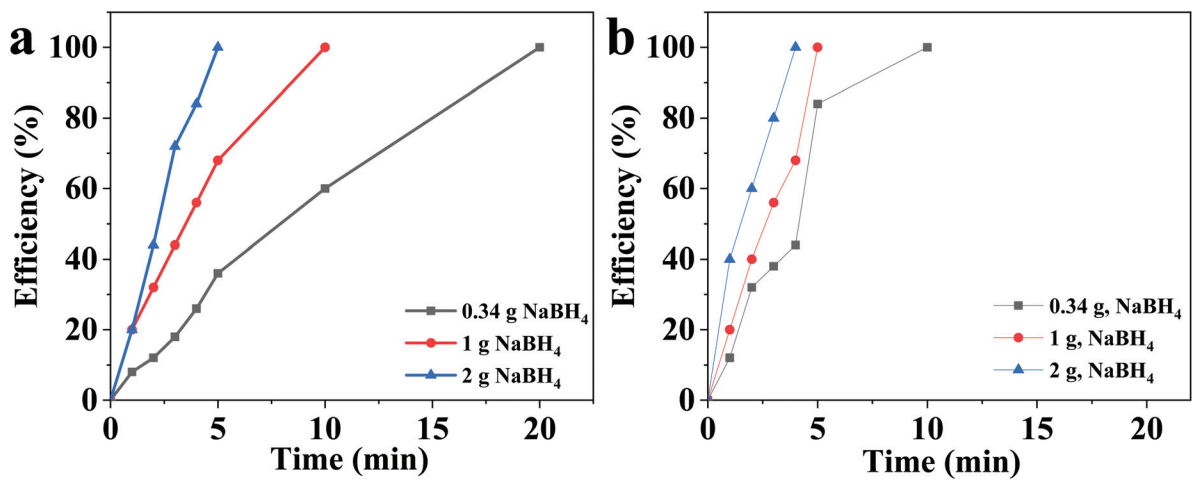

Fig. 6 The efficiency of the hydrolysis at a temperature of (a) 50 °C and 60 °C using 50 mg of UiO-66.

ated hydrogen increases with time. The time to reach the maximum hydrogen volume *i.e.* 500 mL decreases with the increase of the catalyst loading (Fig. 5). This observation is consistent for different concentrations of $NaBH_4$ (0.19 wt%, 0.3 wt%, 1 wt%, 2 wt%, and 3 wt%). The reaction time decreases with the increase of the $NaBH_4$ loading (Fig. 5a–c). It is also important to note that the rate of hydrogen generation decreases over time (Fig. 5d). This is due to the decrease in the concentration of $NaBH_4$ in the solution with time (Fig. 5d). The maximum and average hydrogen generation rates (HGR)

Table 1 Summary of some MOFs which were used as catalysts for hydrogen generation *via* the hydrolysis of $NaBH_4$

Catalysts	Synthesis conditions	Reaction conditions					
		Cat (mg)	$NaBH_4$ (wt%)	NaOH (wt%)	*T* (°C)	HGR (mL min^{-1} g^{-1})	Ref.
CuBDC	Solvothermal, 100 °C for 5h	50	0.05 M	No	25	7620	20
CuO@C	Carbonization at 600 °C for 3 h					7240	
Pd/PD-ZIF-67	Precipitation method, calcination at 200 °C in H_2 atmosphere for 2 h	10	150 mM	0.4		20.6×10^6	19
CoB@ZIF-8	Solvothermal-reduction using $NaBH_4$		1.67	5	35	453.6	45
ZIF-9	Solvothermal method	75	0.5		40	3642	46
ZIF-8	Room temperature	100	0.19	No	30	3000	16
TPA@ZIF-8						2333	18
UiO-66	Solvothermal method, 120 °C for 12h	5	2			6200	This study

Notes: TPA, terephthalic acid.

were 12400 mL min^{-1} g^{-1}, and 6200 mL min^{-1} g^{-1}, respectively (Fig. 5d).

The effect of temperature was also investigated at temperatures of 30 °C (Fig. 5c), 50 °C, and 60 °C (Fig. 6a and b) and with different amounts of $NaBH_4$ with 50 mg of UiO-66. The reaction time to reach the maximum efficiency decreases with an increase of the temperature (Fig. 6a and b). The increase of the efficiency with the increase in the temperature is due to an increase in the kinetics of the reactants and the diffusion rate of the generated gas. The reaction time also decreases with an increase of the amount of $NaBH_4$ (Fig. 6a and b). This effect is due to the increase in the collision between the reactants. Both the temperature and $NaBH_4$ amount can increase the amount of the generated hydrogen gas.

A comparison among different MOFs which were reported as catalysts for the hydrogen generation *via* the hydrolysis of $NaBH_4$ is tabulated in Table 1. The UiO-66 crystals were used as a support for NiFePd.[35] NiFePd@UiO-66 was used as a catalyst for the generation of hydrogen from hydrous hydrazine in an alkaline solution.[35] CuBDC and CuO@C exhibited a HGR of 7620 mL min^{-1} g^{-1} and 7240 mL min^{-1} g^{-1}, respectively.[20] However, CuBDC is a water unstable framework.[43] $NaBH_4$ could also reduce CuO@C to a mixture of Cu_2O and Cu(0).[44] Thus, a calcination step is required to regenerate the catalyst. Partially decomposed ZIF-67 supported Pd nanoclusters (Pd/PD-ZIF-67) were applied for the hydrolysis of $NaBH_4$.[19] The material showed a high HGR. However, it contains expensive noble metals *i.e.* Pd. UiO-66 showed a higher HGR compared to ZIF-based catalysts.[16,18,45,46] The UiO-66 catalyst offers several advantages including a high HGR, simple synthesis procedure, and low cost (Table 1). $NaBH_4$ showed no effect on UiO-66 crystals, thus it can be used as a reducing agent for metals such as Ru.[38] This suggests that UiO-66 can be used as a support for metal nanoparticles for the generation of hydrogen from hydrous hydrazine (NiFePd@UiO-66)[35] or by the hydrolysis of $NaBH_4$.

Conclusion

The solvothermal synthesis of UiO-66 offered an effective catalyst for the generation of hydrogen *via* the hydrolysis of $NaBH_4$. The large surface areas and acidic sites of UiO-66 ensure the high catalytic performance for the hydrolysis of $NaBH_4$. The hydrogen generation rate increases with the increase of the $NaBH_4$ loading. UiO-66 showed an average hydrogen generation rate (HGR) of 6200 mL min^{-1} g^{-1}. It showed a high HGR compared to other MOF-based catalysts. It showed several advantages such as a high HGR, simple synthesis procedure, and low cost. These results may open new avenues for further exploration of an effective catalyst for hydrogen generation *via* the hydrolysis of $NaBH_4$ using MOFs as catalysts.

Conflicts of interest

There are no conflicts to declare.

Acknowledgements

The author would like to thank the Ministry of Higher Education and Scientific Research (Egypt) and Institutional Review Board (IRB) of the Faculty of Science at Assiut University, Egypt, for the support.

References

1 K. Bolatkhan, B. D. Kossalbayev, B. K. Zayadan, T. Tomo, T. N. Veziroglu and S. I. Allakhverdiev, *Int. J. Hydrogen Energy*, 2019, **44**, 5799–5811.
2 N. Srivastava, M. Srivastava, P. K. Mishra, M. A. Kausar, M. Saeed, V. K. Gupta, R. Singh and P. W. Ramteke, *Bioresour. Technol.*, 2020, **307**, 123094.
3 T. da Silva Veras, T. S. Mozer, D. da Costa Rubim Messeder dos Santos and A. da Silva César, *Int. J. Hydrogen Energy*, 2017, **42**, 2018–2033.
4 S. Z. Baykara, *Int. J. Hydrogen Energy*, 2018, **43**, 10605–10614.
5 M. N. Iqbal, A. F. Abdel-Magied, H. N. Abdelhamid, P. Olsén, A. Shatskiy, X. Zou, B. Åkermark, M. D. Kärkäs

and E. V. Johnston, *ACS Sustainable Chem. Eng.*, 2017, **5**, 9651–9656.
6 S. S. Muir and X. Yao, *Int. J. Hydrogen Energy*, 2011, **36**, 5983–5997.
7 L. E. Kreno, K. Leong, O. K. Farha, M. Allendorf, R. P. Van Duyne and J. T. Hupp, *Chem. Rev.*, 2012, **112**, 1105–1125.
8 H.-C. Zhou, J. R. Long and O. M. Yaghi, *Chem. Rev.*, 2012, **112**, 673–674.
9 H. N. Abdelhamid and H.-F. Wu, *J. Mater. Chem. B*, 2013, **1**, 3950–3961.
10 H. N. Abdelhamid, *Lanthanide metal-organic frameworks and hierarchical porous zeolitic imidazolate frameworks: synthesis, properties, and applications*, Stockholm University, Faculty of Science, 2017.
11 H. N. Abdelhamid, *J. Environ. Chem. Eng.*, 2020, **8**, 104008.
12 H. N. Abdelhamid, M. Dowaidar and Ü. Langel, *Microporous Mesoporous Mater.*, 2020, 110200.
13 H. N. Abdelhamid, M. Dowaidar, M. Hällbrink and Ü. Langel, *SSRN Electron., J.*, 2019, DOI: 10.2139/ssrn.3435895.
14 V. R. Bakuru, M. E. DMello and S. B. Kalidindi, *ChemPhysChem*, 2019, **20**, 1177–1215.
15 B. Zhu, R. Zou and Q. Xu, *Adv. Energy Mater.*, 2018, **8**, 1801193.
16 H. N. Abdelhamid, *Macromol. Chem. Phys.*, 2020, **221**, 2000031.
17 H. N. Abdelhamid, *Mater. Today Chem.*, 2020, **15**, 100222.
18 H. N. Abdelhamid, *Dalton Trans.*, 2020, **49**, 4416–4424.
19 C. Wu, J. Guo, J. Zhang, Y. Zhao, J. Tian, T. T. Isimjan and X. Yang, *Renewable Energy*, 2019, **136**, 1064–1070.
20 A. A. Kassem, H. N. Abdelhamid, D. M. Fouad and S. A. Ibrahim, *Int. J. Hydrogen Energy*, 2019, **44**, 31230–31238.
21 J. Winarta, B. Shan, S. M. Mcintyre, L. Ye, C. Wang, J. Liu and B. Mu, *Cryst. Growth Des.*, 2020, **20**, 1347–1362.
22 J. H. Cavka, S. Jakobsen, U. Olsbye, N. Guillou, C. Lamberti, S. Bordiga and K. P. Lillerud, *J. Am. Chem. Soc.*, 2008, **130**, 13850–13851.
23 C. Atzori, K. A. Lomachenko, J. Jacobsen, N. Stock, A. Damin, F. Bonino and S. Bordiga, *Dalton Trans.*, 2020, **49**, 5794–5797.
24 S. Seth, T. P. Vaid and A. J. Matzger, *Dalton Trans.*, 2019, **48**, 13483–13490.
25 Y. Pan, Z. Luo, X. Wang, Q. Chen, J. Chen, Y. Guan, D. Liu, H. Xu and J. Liu, *Dalton Trans.*, 2020, **49**, 5291–5301.
26 S.-X. Lin, W.-L. Pan, R.-J. Niu, Y. Liu, J.-X. Chen, W.-H. Zhang, J.-P. Lang and D. J. Young, *Dalton Trans.*, 2019, **48**, 5308–5314.
27 A. Koutsianos, E. Kazimierska, A. R. Barron, M. Taddei and E. Andreoli, *Dalton Trans.*, 2019, **48**, 3349–3359.
28 N. Shokouhfar, L. Aboutorabi and A. Morsali, *Dalton Trans.*, 2018, **47**, 14549–14555.
29 Y. Yang, Z. Niu, H. Li, Y. Ma, Y. Zhang and H. Wang, *Dalton Trans.*, 2018, **47**, 6538–6548.
30 S. Das and T. Ben, *Dalton Trans.*, 2018, **47**, 7206–7212.
31 M. SK, M. R. U. Khan, A. Das, S. Nandi, V. Trivedi and S. Biswas, *Dalton Trans.*, 2019, **48**, 12615–12621.
32 V. R. Bakuru, D. Samanta, T. K. Maji and S. B. Kalidindi, *Dalton Trans.*, 2020, **49**, 5024–5028.
33 M. Bhattacharya, K. J. Chandler, J. Geary and C. T. Saouma, *Dalton Trans.*, 2020, **49**, 4751–4757.
34 V. R. Bakuru, D. Davis and S. B. Kalidindi, *Dalton Trans.*, 2019, **48**, 8573–8577.
35 X. Song, P. Yang, J. Wang, X. Zhao, Y. Zhou, Y. Li and L. Yang, *Inorg. Chem. Front.*, 2019, **6**, 2727–2735.
36 A. R. Abdellah, H. N. Abdelhamid, A.-B. A. A. M. El-Adasy, A. A. Atalla and K. I. Aly, *J. Environ. Chem. Eng.*, 2020, **8**, 104054.
37 A. K. Ghosh, S. Paul, P. Sood, S. M. Rudramurthy, A. Rajbanshi, T. J. Jillwin and A. Chakrabarti, *Clin. Microbiol. Infect.*, 2015, **21**, 372–378.
38 Q. Yang, H.-Y. Zhang, L. Wang, Y. Zhang and J. Zhao, *ACS Omega*, 2018, **3**, 4199–4212.
39 M. N. Goda, H. N. Abdelhamid and A.-A. Said, *ACS Appl. Mater. Interfaces*, 2020, **12**, 646–653.
40 L. Valenzano, B. Civalleri, S. Chavan, S. Bordiga, M. H. Nilsen, S. Jakobsen, K. P. Lillerud and C. Lamberti, *Chem. Mater.*, 2011, **23**, 1700–1718.
41 J. Hajek, B. Bueken, M. Waroquier, D. De Vos and V. Van Speybroeck, *ChemCatChem*, 2017, **9**, 2203–2210.
42 C. D. Fast, J. Woods, J. Lentchner and T. A. Makal, *Dalton Trans.*, 2019, **48**, 14696–14704.
43 H. N. Abdelhamid, *Nanotechnology*, 2019, **30**, 435601.
44 A. A. Kassem, H. N. Abdelhamid, D. M. Fouad and S. A. Ibrahim, *Microporous Mesoporous Mater.*, 2020, **305**, 110340.
45 Q. Li, W. Yang, F. Li, A. Cui and J. Hong, *Int. J. Hydrogen Energy*, 2018, **43**, 271–282.
46 Q. Li and H. Kim, *Fuel Process. Technol.*, 2012, **100**, 43–48.